

Well-Dispersed Ru-Clusters Decorating Nanobox-Structured CoP Synergistically Catalyze the NaBH₄ Hydrolysis and Electro-Reductive H₂ Evolution

Shasha Dou⁺,^[a] Chuan Hu⁺,^[a] Luyan Shi,^[a] Wanyu Zhang,^[a] Shuqing Zhou,^[a] Puxuan Yan,^[a] Lawrence D'Souza,^[b] Tayirjan Taylor Isimjan,^{*,[b]} and Xiulin Yang^{*,[a]}

The high-efficiency multifunctional materials have considerable significance in the area of sustainable energy to developing a cross-usable and low-cost catalyst. Nevertheless, substantial challenges are ahead on designing and synthesizing a high performance in a scalable and straightforward manner. Here, we have developed a novel bifunctional catalyst based on Ru/CoP nanoboxes (NBs) prepared using ZIF-67 as a precursor. The nano hollow box structure and the strong electronic interaction between Ru clusters and CoP component are confirmed. The Ru/CoP NBs as a catalyst show excellent activities for catalytic

NaBH₄ hydrolysis such as high turnover frequency (1202.2 min⁻¹), and small electrocatalytic H₂ evolution overpotential (49 mV@10 mAcm⁻²) under ambient conditions. Besides, Ru/CoP NBs also display good stability and reusability. The excellent catalytic performance of Ru/CoP NBs is attributed to the synergy between Ru clusters and CoP species as well as the unique morphology that accelerates charge transfer, provides higher active surface area, and facilitates solute transport and gas emission.

1. Introduction

The synergy between structure and composition determines the physical/chemical properties of materials.^[1] Due to the unique structural features, hollow-structure carbon composite materials have attracted widespread attention in the fields of catalysis, energy storage, and controlled release because of their large surface area, high electrical conductivity, high availability, and low cost.^[2] Until the last century, hollow structural materials could only be synthesized on the macro and micro scales by spray drying, air blowing, and other methods.^[3] Since then, the template method has been slowly merging into the general synthetic paradigm for hollow structures owing to its advantages in controlling morphologies, physical, and chemical properties.^[4] Along with this line, many new physical and chemical strategies have been studied to prepare hollow carbon materials, such as template-assisted assembly,^[5] self-assembly,^[6] chemical etching,^[7] and electroplating replacement.^[8] However, it has always been a challenge to synthesize porous/ hole structure materials with specific

components in a controlled manner.^[9] As an emerging material, metal-organic frameworks (MOFs) have been attracted a lot of attention owing to their unique structural properties (adjustable porosity and geometric shapes) associated with various functions, including energy storage, chemical separation & purification, catalysis, and sensing.^[10] Furthermore, MOFs have shown great potential as precursors for constructing multifunctional carbon-based organic/inorganic hybrid materials.^[11] Especially, MOFs precursors have demonstrated great potential in synthesizing various hollow structural materials with adjustable porosity, diverse morphology, graded/multi-shell structure, multiple internal cavities/channels, etc. for the electrochemical form of energy storage.^[10b,12] The MOF based hollow materials can be prepared in various ways, such as template-mediated assembly, interface synthesis, chemical etching, ion exchange reaction, and heat treatment.^[13]

As a clean alternative energy source, the green hydrogen can be produced either by sustainable electrochemical water splitting^[14] or by hydrolysis of metal hydrides considered hydrogen storage molecules.^[15] Due to the sluggish kinetics, the metal hydride hydrolysis requires catalysts to accelerate the reaction rate. In general, the metal hydrides needs to be dissolved in the alkaline media, and the hydrogen generation starts upon the addition of the catalyst. The leftover alkaline solution can be subjected to direct electrolysis after the hydrolysis process to produce hydrogen until all the water is consumed. This method is especially useful in places facing severe water shortages. As a result, it would be convenient if the catalyst has double functions such as metal hydride hydrolysis and hydrogen evaluation reaction (HER). Series of such bifunctional catalysts on various supports have been developed recently. Most of these kinds of catalysts are based on Pt,^[16] but they are limited by the Pt's high price and scarcity.

[a] S. Dou,⁺ C. Hu,⁺ L. Shi, W. Zhang, S. Zhou, P. Yan, Prof. X. Yang
Guangxi Key Laboratory of Low Carbon Energy Materials
School of Chemistry and Pharmaceutical Sciences
Guangxi Normal University
Guilin 541004 (P. R. China)
E-mail: xlyang@gxnu.edu.cn

[b] Dr. L. D'Souza, Dr. T. T. Isimjan
Saudi Arabia Basic Industries Corporation (SABIC)
at King Abdullah University of Science and Technology (KAUST)
Thuwal 23955-6900 (Saudi Arabia)
E-mail: isimjant@sabic.com

[⁺] These authors contributed equally to this work.

 Supporting information for this article is available on the WWW under <https://doi.org/10.1002/cctc.202100768>

Therefore, Pt free bifunctional catalysts are often preferred. Recently, we reported a rugae-like bifunctional catalyst of Ni₂P–CoP nanoarrays.^[17] We conclude that the outstanding performance is attributed to the synergistic effect between Ni and Co and a unique morphology resulting in better mass transfer. However, there is still room for further improvement. Our previous experience shows that the addition of trace amounts of Ru to the base catalyst could significantly improve the catalyst performance and offer a better price balance.^[15a]

As a continuation of our previous study, we report a rational design and synthesis of Ru nanoclusters modified carbon nanoboxes containing Co metal phosphides (denoted as Ru/CoP NBs) through the MOF template strategy. The results revealed that the unique hollow nanostructure feature enriches active sites and increases the accessible surface area that improves the mass transfer process. At the same time, the synergy between Ru and CoP species significantly enhances the catalytic performance. The optimized Ru/CoP NBs displayed NaBH₄ hydrolysis with a high turnover frequency (1202.2 min⁻¹) and a low HER overpotential (49 mV@10 mA cm⁻²) in 0.5 M H₂SO₄.

Experimental

Synthesis of ZIF-67 nanocubes

In a typical synthesis, 580 mg of Co(NO₃)₂·6H₂O was dissolved in 20 mL of deionized water containing 10 mg of cetrimonium bromide (CTAB).^[18] Then this solution was rapidly injected into 140 mL of an aqueous solution containing 908 mg of 2-methylimidazole and stirred at room temperature for 30 min. The resulted precipitate was collected by centrifugation, washed three times with abundant ethanol, and vacuum-dried at 70 °C for 12 hours. The resulting product was named ZIF-67 nanocubes (NCs).

Synthesis of Co LDH@ZIF-67 NCs

First, 100 mg of ZIF-67 NCs was dispersed into 60 mL of ethanol. Then 10 mL of ethanol solution containing 300 mg Co(NO₃)₂·6H₂O was added and stirred for 1 min. The reaction vessel was then put into an ultrasonic bath for 40 min. Finally, the product was washed by ethanol several times and dried at 70 °C overnight. The collected sample was Co LDH@ZIF-67 NCs.

Synthesis of Co LDH NBs

The ZIF-67 in the Co LDH@ZIF-67 NCs needs to be removed to obtain pure Co LDH NBs. First, 200 mg of the Co LDH@ZIF-67 NCs was dispersed in 60 mL of deionized water. The mixed solution was heated to 80 °C for 10 min, during which the ZIF-67 can be removed entirely, indicated by the disappearance of purple color. The product was then washed several times with ethanol and dried overnight at 70 °C. The resulting sample was named as Co LDH NBs.

Synthesis of CoP NBs and CoP NCs

The as-prepared Co LDH NBs were further annealed with NaH₂PO₂ at 350 °C for 2 h with a ramp rate of 5 °C min⁻¹ under a flow of nitrogen gas. The resulted product was nominated as CoP NBs. For

comparison, CoP NCs was obtained by directly phosphating Co LDH@ZIF-67 NCs using a similar method as discussed above.

Synthesis of Ru/CoP NBs

Typically, 30 mg CoP NBs and different masses of RuCl₃·3H₂O were ultrasonically dispersed into 15 mL H₂O to form a homogeneous suspension. After continuous stirring for 5 h, 2 mL of 0.6 M NaBH₄ solution was added dropwise into the above mixture. Thirty minutes later, the resulted black precipitate was centrifuged, washed three times with water, and freeze-dried for 12 h to give the final product. Theoretical results show that the mass percentage of Ru in the composite is 1.4~2.7 wt.%, and the catalytic performance is best when the mass percentage of Ru is 2.1 wt.%. As a comparison, a mass ratio of 2.1 wt.% Ru was applied to synthesize all other control catalysts. Notably, all the synthetic processes were described above besides that the mass of the RuCl₃·3H₂O was fixed at 8.0 mg, and the support was replaced with CoP NCs, and XC-72 carbon black, respectively. The obtained catalysts were nominated as Ru/CoP NCs, and Ru/CB, respectively.

Catalytic hydrolysis for H₂ generation

The catalytic hydrolysis of NaBH₄ to produce hydrogen is as follows. Firstly, a solution of 50 mL 150 mM NaBH₄+0.4 w.% NaOH is poured into a 100 mL three-neck-bottom flask and stirred at 25 °C for 30 min in a thermostatic water bath until no gas is discharged. The electronic balance weighs the quality of the water released from the drainage collection bottle. Secondly, 10 mg catalyst was weighed and added to the above reaction bottle. The discharge water mass was immediately recorded by an electronic balance (Note: Connect with a computer to record data in real-time). Thirdly, the stability test is to add fresh NaBH₄ powder to the remaining liquid of the last experiment (Note: make sure that the last reaction is complete before proceeding to the next experiment). Finally, the apparent activation energy (E_a) is obtained by continuously adjusting the reaction temperature (298~318 K) of the thermostatic water bath to test the NaBH₄ hydrolysis reaction.

Electrochemical hydrogen evolution studies

Electrochemical reaction was carried out on a typical multi-channel three-electrode electrochemical workstation (Biologic VMP3, France) with a saturated calomel electrode (SCE) and graphite plate as a reference and counter electrodes, respectively. The carbon cloth (CC) modified by the catalyst powder is used as the working electrode. The synthesis method is as follows: Ru/CoP NBs (2 mg) was first dispersed in 0.5 mL isopropanol, and then 25 μL Nafion (5%) was added to the solution, followed by ultrasonic treatment for 1 h. After that, 52 μL of the inks was pipetted onto the CC surface (1.0 cm²) and dried naturally. As a control, we simultaneously loaded CoP NBs, Ru/CB, and Pt/C materials on the surface of CC to obtain different control catalysts.

In the electrochemical test, we first perform cyclic voltammetry (3~5 cycles) to stabilize the catalytic performance of the catalyst (20 mVs⁻¹), followed by test the linear sweep voltammetry (LSV) curve at a scan rate of 20 mVs⁻¹ and electrochemical impedance spectroscopy (EIS) in the frequency range of 200 kHz to 10 mHz. The electrochemical double-layer capacitance (C_{dl}) was obtained by CV method with different scan rates measured in a non-Faraday potential regions. All potentials in this work are calibrated to RHE using the average CV curves of the two potentials at the current crossing zero (0.244 V) as thermodynamic potentials in H₂-saturated 0.5 M H₂SO₄ (Figure S7). All tests are performed at an ambient

temperature of approximately 25 °C, and all the curves discussed below have been *iR*-corrected.

2. Results and discussion

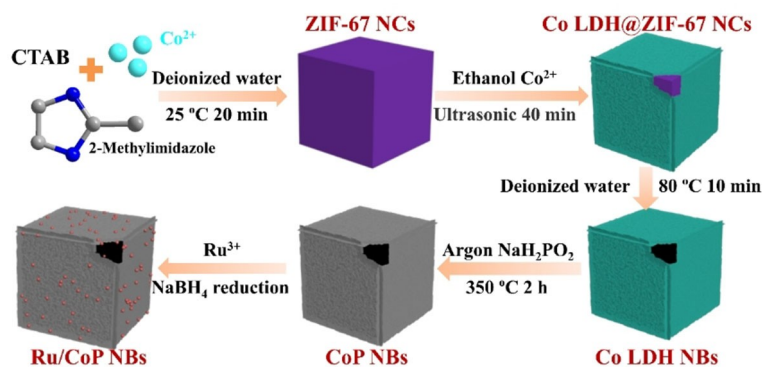
2.1. Synthetic strategy analysis

The schematic diagram of the five-step preparation method of Ru/CoP NBs composite is shown in Scheme 1. Step 1: Co-based ZIF-67 NCs with uniform morphology are synthesized by a surfactant-mediation method. Step 2: the Co-layered hydroxide (LDH) covered ZIF-67 NCs (Co LDH@ZIF-67) was prepared by ultrasonically mixing the ZIF-67 NCs with Co(NO₃)₂ at room temperature. Step 3: the Co LDH@ZIF-67 NCs was added to deionized water at 80 °C to remove the ZIF-67 template, thereby preparing Co LDH NBs. During the process, the inner part of

ZIF-67 diffused out of the nanocubes to form Co LDH NBs. Step 4: the Co LDH NBs are chemically converted into Co metal phosphides by treatment with NaH₂PO₂ at 350 °C for 2 h under nitrogen atmosphere. Step 5: the Ru clusters were loaded on the CoP NBs substrate with NaBH₄ as the reducing agent. ICP-AES determined the actual Ru loading, and the result was used to calculate the HGR and TOF values (Table S1). Similarly, the rest of the controls were performed.

2.2. Microstructure and crystallinity analysis

The morphology of the synthesized nanocrystals was initially characterized by scanning electron microscopy (SEM). The SEM image (Figure 1a) shows that the synthesized ZIF-67 is a uniform cubic structure with a smooth surface and a size of about 400 nm. After treating with a Co(NO₃)₂ for 40 min at



Scheme 1. Schematic diagram of the synthesis of Ru/CoP NBs composite.

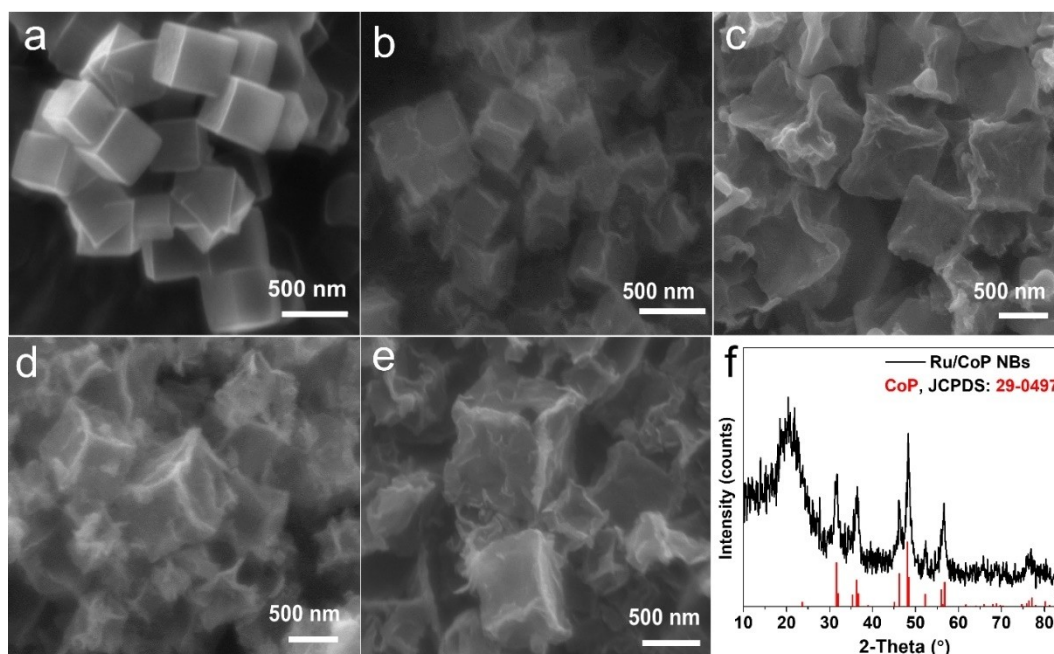


Figure 1. SEM images of (a) ZIF-67 NCs, (b) Co LDH@ZIF-67 NCs, (c) Co LDH NBs, (d) CoP NBs and (e) Ru/CoP NBs. (f) XRD pattern of Ru/CoP NBs.

room temperature, the solid ZIF-67 NCs were converted into Co LDH@ZIF-67 NCs (Figure 1b). The XRD pattern shows the characteristic peak of ZIF-67 along with some diffraction peaks of Co LDH (Figure S1a).^[19] When Co LDH@ZIF-67 NCs were treated at 80 °C for 10 min, the ZIF-67 species were selectively removed (Figure 1c), which was also confirmed by XRD (Figure S1b).^[20] The chemical transformation between different species can be observed through thermogravimetric (TG) analysis where the exothermic peaks at 529 and 483 °C belong to the pyrolysis of ZIF-67 and the exothermic peaks at 221 and 193 °C are due to the dehydration of Co LDH (Figure S2). Figure 1d reveals that the Co LDH NBs phosphorization does not change the overall structure of the NBs, and the cubic NBs still kept the cavity and a porous wall structure. The purpose of the LDH is to improve the Co dispersion, which was realized using high surface area cubic ZIF-67 as a template. Through this transformation, the solid cube material was transformed into a hollow nanobox, thus significantly improving the dispersion of the Co species throughout the cubic structure. The nanobox-like structure was retained (Figure 1e) after the loading Ru clusters. XRD cannot detect the Ru clusters due to the low loading of Ru (Figure 1f).^[17,21]

As shown in Figure 2a, transmission electron microscope (TEM) images show that ZIF-67 exhibits sharp edges and a well-defined cube structure. After reacting with an appropriate amount of Co (NO₃)₂ for 40 min at room temperature, sheet-like folds are formed on the surface and further etched into hollow structures. The solid ZIF-67 NCs were converted into Co LDH@ZIF-67 NCs (Figure 2b). As shown in Figure 2c, after removing the ZIF-67 template, the morphology did not change much. Figure 2d clearly shows the cavity inside the cubical nanoboxes and the porous structure of the walls. Meanwhile, the high-resolution TEM image of Ru/CoP NBs (Figure 2e) shows

two different cross lattice fringes with a plane spacing of 0.28 nm and 0.38 nm, which correspond to the (011) and (101) planes of CoP, respectively.^[22] The EDX spectrum of Ru/CoP NBs confirms the presence of Ru, Co, P, O, and C in the material (Figure S3). Furthermore, the HAADF-STEM and the elemental mappings show that Co, Ru, and P elements are uniformly distributed on the edges of Ru/CoP NBs (Figure 2f).

2.3. XPS analysis

The composition and chemical state of Ru/CoP NBs, Ru/CB, and CoP NBs were studied by X-ray photoelectron spectroscopy (XPS). The elemental surveys of both samples are shown in Figure S4. The high-resolution XPS spectrum of the C 1s used as calibration standard was deconvoluted into C=C (284.0 eV), C–C (284.8 eV), and C–O (286.0 eV),^[23] and the Ru 3d_{5/2} core level was deconvoluted at the binding energies of 280.0 eV (metallic Ru) and 281.5 eV (Ru oxide)^[24] as shown in Figure 3a. It is worth noting that there are only metallic Ru species in Ru/CB, while there are both metallic Ru and high-valence Ru oxide species in Ru/CoP NBs. Moreover, the metallic Ru is positively shifted by 0.75 eV compared with Ru/CB, indicating a strong interaction between Ru species and CoP species. Figure 3b shows the high-resolution Co 2p spectra of Ru/CoP NBs and CoP NBs. The Co 2p_{3/2} region is equipped with three peaks at 777.9, 780.7, and 784.7 eV, which correspond to the Co–P, Co–O, and satellite peaks.^[25] Notably, in Co 2p, almost no shift is observed because of Ru's trace amount. Therefore, amounts of the electrons transferred from Ru to Co are not enough to cause a noticeable change on Co 2p binding energy. Besides, the high-resolution XPS spectrum of the P 2p core level shows three types of peaks (Figure 3c), where a pair of peaks located at 128.8 eV (P 2p_{3/2})

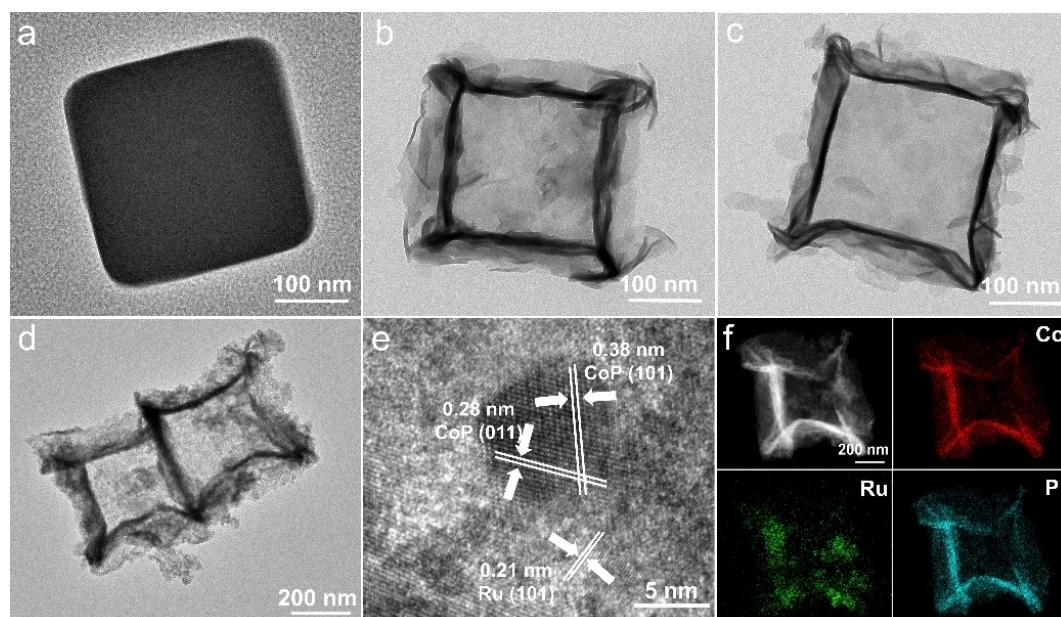


Figure 2. TEM images of (a) ZIF-67 NCs, (b) Co LDH@ZIF-67 NCs, and (c) Co LDH NBs. (d) TEM and (e) high-resolution TEM images of Ru/CoP NBs. (f) HAADF-STEM image of Ru/CoP NBs and corresponding element mappings of Co, Ru and P.

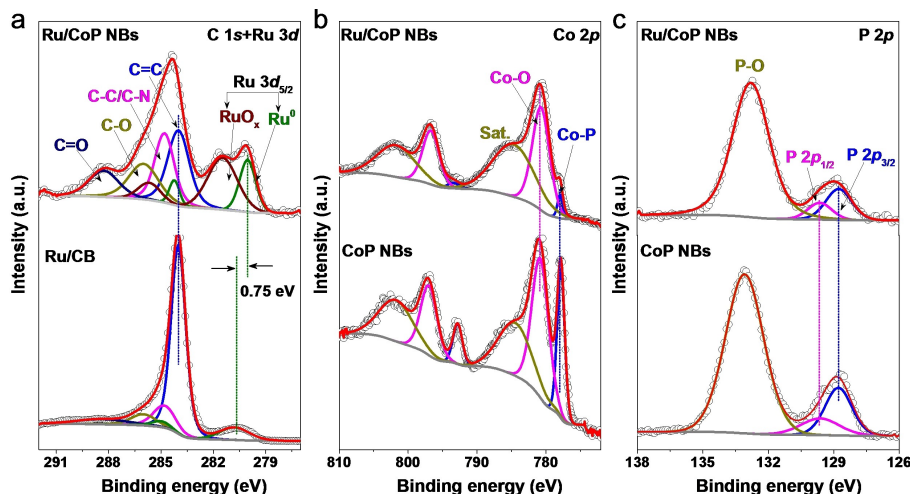


Figure 3. High-resolution X-ray photoelectron spectroscopy (XPS) of (a) C 1s+Ru 3d, (b) Co 2p and (c) P 2p regions from Ru/CoP NBs, Ru/CB and CoP NBs.

and 129.7 eV ($P\ 2p_{1/2}$) are attributed to P 2p in CoP.^[22c] There is a broad peak associated with phosphorus oxide at 132.8 eV. Studies have found that these prominent oxidation peaks of Co–O and P–O are caused by unavoidable surface oxidation.^[26] The remarkable electron transfer characteristics and unique surface chemical-state species are the key factors to improve the catalytic performance significantly, as discussed below.

2.4. Catalytic NaBH_4 hydrolysis

The catalytic hydrolysis of sodium borohydride is carried out in an alkalinized NaBH_4 solution at 25 °C. The amount of H_2 produced was calculated from the amount of water replaced by H_2 (Figure S5). According to the catalytic performance, the Ru loading was optimized, as shown in Figure 4a. The results show that the H_2 production rate increases with the increase in Ru content up to the Ru loading of 2.1 wt.%, and subsequently showed the highest TOF value (Figure 4b). Therefore, 2.1 wt.% Ru loading was kept during the rest of the optimization processes. Various supports were used at the same Ru loading

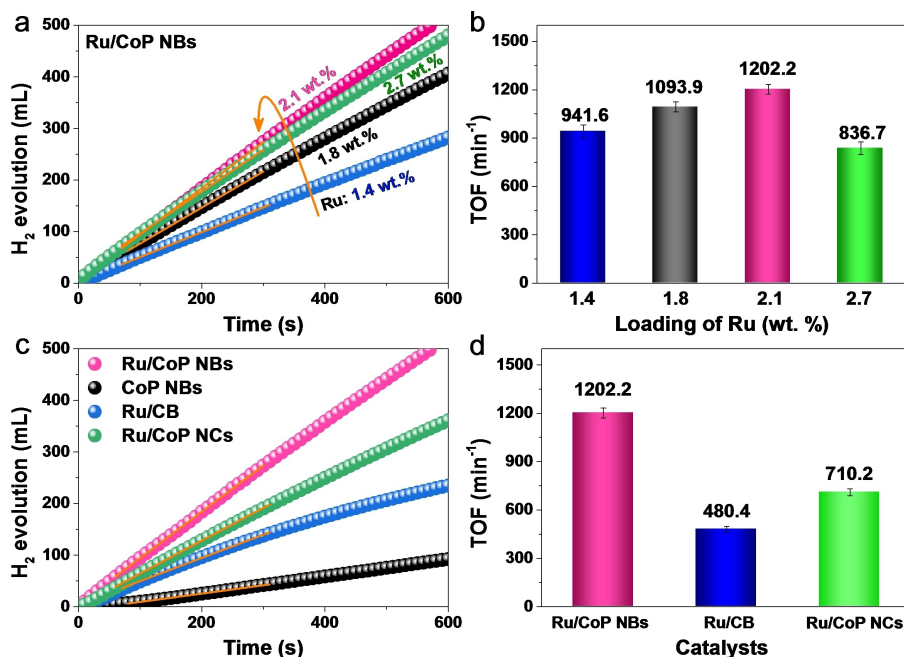


Figure 4. (a) The relationship between the H_2 generation rates and loadings of Ru species on Ru/CoP NBs catalysts, and (b) the summarized TOF values. (c) Stoichiometric H_2 evolution and (d) the summarized TOF values of different catalysts (2.1 wt.% Ru) in 150 mM NaBH_4 + 0.4 wt.% NaOH solution at 25 °C.

to evaluate the support effect on the catalytic performance (2.1 wt.%). The Ru/CoP NBs was significantly higher in catalytic activity than Ru-loaded CoP NCs and all other control catalysts (Figure 4c). Figure 4d shows that the TOF value of Ru/CoP NBs is 1202.2 min^{-1} (moles of Ru in the hybrid catalyst), which is higher than these of Ru/CB and Ru/CoP NCs and also superior to most previously reported catalysts (Table S2).

To measure the activation energy of Ru/CoP NBs, a set of experiments were carried out at different temperatures (Figure 5a). As the reaction temperature increases from 298 K to 318 K, the H_2 generation rate (HGR) increases rapidly, and the rate constant κ is calculated based on the slope of each experiment. According to the Arrhenius diagram ($\ln \kappa$ vs. $1/T$), the activation energy of the Ru/CoP NBs catalyst is estimated to be 42.6 kJ mol^{-1} (Figure 5b), slightly lower than CoP NBs (Figure S6), implying the fastest kinetics of NaBH_4 hydrolysis. The continuous cycling test is used to evaluate Ru/CoP NBs catalyst's stability and reusability in sodium borohydride alkaline solution (Figure 5c). The results show that the Ru/CoP NBs catalyst has an excellent recovery capacity for catalytic hydrogen production. After the fifth cycle, it retained about 73.6% of its initial catalytic capacity (Figure 5d). The slight decrease in catalytic activity may be due to the spalling of Ru species (after five cycles, the mass fraction of Ru species was reduced to 1.8 wt.% by ICP, Table S1), structural damage, and catalyst poisoning.^[15b,17]

2.5. Electrocatalytic hydrogen evolution

Apart from the catalytic NaBH_4 hydrolysis, HER performance of the Ru/CoP NBs was also measured in a 0.5 M H_2SO_4 solution. The HER results were corrected to the RHE potential, and the calibration parameter was obtained in an H_2 saturated electrolyte (Figure S7). For comparison, control experiments using CoP NBs, Ru/CB, Pt/C, and carbon cloth as electrocatalysts for the HER were also performed. As shown in Figure 6a, the Ru/CoP NBs has the second-best electrolytic activity next to 20% Pt/C. The overpotential at 10 mA cm^{-2} is 49 mV, which is significantly lower than that of CoP NBs ($\eta_{10} = 115 \text{ mV}$), Ru/CB ($\eta_{10} = 93 \text{ mV}$), and part of the previously reported Ru-based catalysts (Table S3). The results reveal that this excellent electrocatalytic activity is the outcome of the unique synergy between the Ru and CoP components since Ru/CoP NBs have much better performance than those of CoP NBs, Ru/CB, and CC. Moreover, as shown in Figure 6b, the Tafel slope of Ru/CoP NBs was calculated as about 28.8 mV dec^{-1} , which is lower than that of CoP NBs ($109.8 \text{ mV dec}^{-1}$), Ru/CB (43.5 mV dec^{-1}), indicating that the Volmer-Tafel reaction pathway with the recombination step is the rate-determining step in acid solution.^[27] Besides, electrochemical double-layer capacitance (C_{dl}), which is linearly proportional to electrochemical surface area (ECSA), was measured by cyclic voltammetry (CV) is from 0.03 to 0.13 V vs. RHE in a non-Faradaic potential region (Figure S8). As shown in Figure 6c, the calculated C_{dl} value of Ru/CoP NBs is 19.0 mF cm^{-2} , higher than all other control catalysts indicating the large ECSA and more catalytically active sites for HER reactions.^[28] Also, electrochemical impedance spectroscopy (EIS) was carried out to study

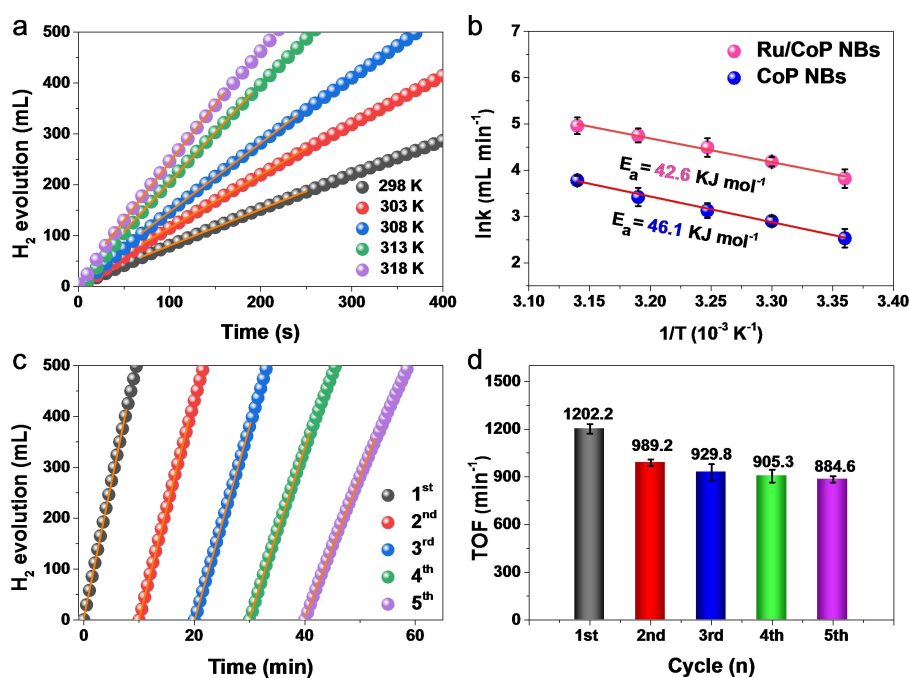


Figure 5. (a) Stoichiometric H_2 evolution of Ru/CoP NBs in 150 mM $\text{NaBH}_4 + 0.4 \text{ wt. \% NaOH}$ solution at different reaction temperatures, and (b) the summarized Arrhenius plots from (a). (c) Recycling stability test of Ru/CoP NBs catalyst in 150 mM $\text{NaBH}_4 + 0.4 \text{ wt. \% NaOH}$ at 25°C . (d) The summarized TOF values in different recycling test.

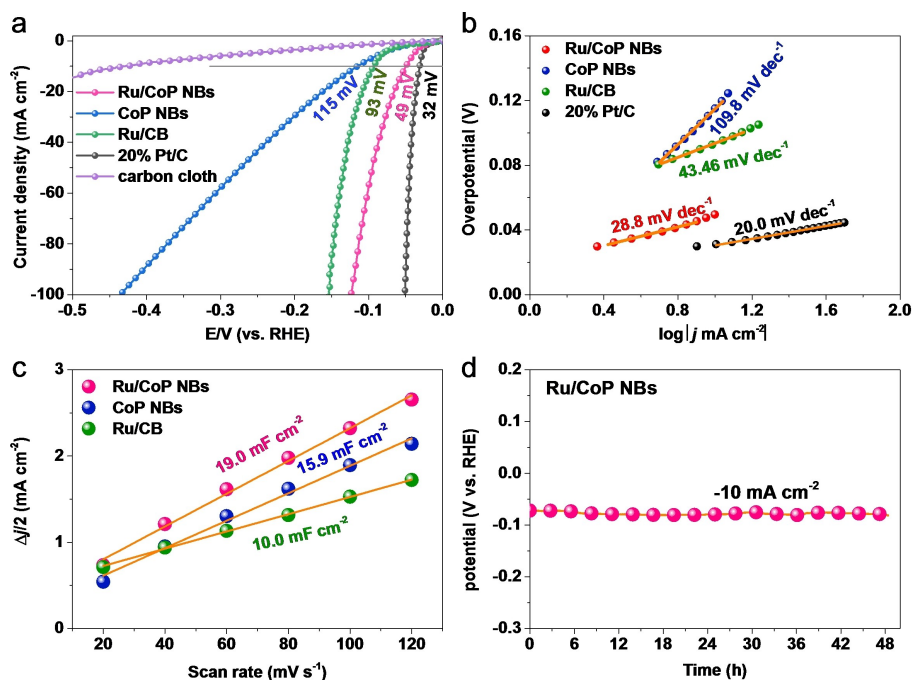


Figure 6. (a) Polarization curves and (b) Tafel plots of Ru/CoP NBs, CoP NBs, Ru/CB, Pt/C and carbon cloth. All the measurements are carried out in 0.5 M H₂SO₄ at a scan rate of 2 mV s⁻¹. (c) The summarized double-layer capacitance (C_{dl}) of different catalysts. (d) Chronopotentiometric curve of Ru/CoP NBs catalyst at -10 mA cm⁻² for 48 h.

the electrode kinetics under HER condition (Figure S9). The Ru/CoP NBs catalyst has the second-lowest electron transfer impedance next to Pt/C, illustrating faster electron transfer characteristics owing to the high conductivity. Finally, the Ru/CoP NBs catalyst exhibits excellent HER stability within 48 h at a current density of 10 mA cm⁻² (Figure 6d), showing a good prospect for commercial applications.

3. Conclusions

In summary, we have developed a facile metal-organic framework (MOF)-based strategy to synthesize Ru/CoP NBs from ZIF-67 NCs precursors. The resultant Ru/CoP NBs as a catalyst showed excellent activities for catalytic NaBH₄ hydrolysis with a high TOF (1202.2 min⁻¹) and a low electrocatalytic hydrogen evolution potential (η_{10} = 49 mV) under ambient conditions. The Ru/CoP NBs also displayed good stability. The excellent catalytic performance could be due to the high conductivity, strong charge transfer property between Ru and Co species, and large surface area. We believe this work could be an excellent addition to the growing family of MOF-based functional materials that can be used in various fields, including catalysis, fuel cells, and supercapacitors, etc.

Acknowledgments

This work has been supported by the National Natural Science Foundation of China (no. 21965005), Natural Science Founda-

tion of Guangxi Province (2018GXNSFAA294077, 2021GXNSFAA076001), Project of High-Level Talents of Guangxi (F-KA18015), and Guangxi Technology Base and Talent Subject (GUIKE AD18126001, GUIKE AD20297039).

Conflict of Interest

The authors declare no conflict of interest.

Keywords: Ru/CoP nanoboxes · Electron transfer · NaBH₄ hydrolysis · Water splitting · Synergistic catalysis

- [1] a) R. V. Jagadeesh, K. Murugesan, A. S. Alshammari, H. Neumann, M.-M. Pohl, J. Radnik, M. Beller, *Science* **2017**, *358*, 326–332; b) S. S. A. Shah, T. Najam, M. K. Aslam, M. Ashfaq, M. M. Rahman, K. Wang, P. Tsiakaras, S. Song, Y. Wang, *Appl. Catal. B* **2020**, *268*, 118570.
- [2] a) F. Xu, Z. Tang, S. Huang, L. Chen, Y. Liang, W. Mai, H. Zhong, R. Fu, D. Wu, *Nat. Commun.* **2015**, *6*, 7221; b) L. Qin, R. Ru, J. Mao, Q. Meng, Z. Fan, X. Li, G. Zhang, *Appl. Catal. B* **2020**, *269*, 118754; c) L. Zhou, Z. Zhuang, H. Zhao, M. Lin, D. Zhao, L. Mai, *Adv. Mater.* **2017**, *29*, 1602914; d) J. Qi, X. Lai, J. Wang, H. Tang, H. Ren, Y. Yang, Q. Jin, L. Zhang, R. Yu, G. Ma, Z. Su, H. Zhao, D. Wang, *Chem. Soc. Rev.* **2015**, *44*, 6749–6773.
- [3] a) S. Niu, W.-J. Jiang, Z. Wei, T. Tang, J. Ma, J.-S. Hu, L.-J. Wan, *J. Am. Chem. Soc.* **2019**, *141*, 7005–7013; b) Z. Teng, W. Li, Y. Tang, A. Elzathry, G. Lu, D. Zhao, *Adv. Mater.* **2019**, *31*, 1707612; c) J.-S. Park, S. Yang, Y. C. Kang, *Chem. Eng. J.* **2020**, *393*, 124606.
- [4] L. Yang, H. Lv, M. Li, Y. Zhang, J. Liu, Z. Yang, *Chem. Eng. J.* **2020**, *392*, 123666.
- [5] Z. Yang, Z. Niu, Y. Lu, Z. Hu, C. C. Han, *Angew. Chem. Int. Ed.* **2003**, *42*, 1943–1945; *Angew. Chem.* **2003**, *115*, 1987–1989.
- [6] M. Mo, J. C. Yu, L. Zhang, S.-K. A. Li, *Adv. Mater.* **2005**, *17*, 756–760.

- [7] a) Y. Chen, H.-R. Chen, J.-L. Shi, *Acc. Chem. Res.* **2014**, *47*, 125–137; b) L. Wang, Y. Yamauchi, *J. Am. Chem. Soc.* **2013**, *135*, 16762–16765.
- [8] H. Hu, Bu Y. Guan, Xiong W. Lou, *Chem* **2016**, *1*, 102–113.
- [9] a) H.-Y. Chen, H.-J. Niu, Z. Han, J.-J. Feng, H. Huang, A.-J. Wang, *J. Colloid Interface Sci.* **2020**, *570*, 205–211; b) Q. Sun, Z. Cao, S. Wang, L. Sun, L. Zhou, H. Xue, Y. Wu, L. Cavallo, L. Wang, J. Ming, *J. Power Sources* **2020**, *461*, 228128.
- [10] a) J. Li, X. Han, X. Zhang, A. M. Sheveleva, Y. Cheng, F. Tuna, E. J. L. McInnes, L. J. McCormick McPherson, S. J. Teat, L. L. Daemen, A. J. Ramirez-Cuesta, M. Schröder, S. Yang, *Nat. Chem.* **2019**, *11*, 1085–1090; b) S. Lee, S. Oh, M. Oh, *Angew. Chem. Int. Ed.* **2020**, *59*, 1327–1333; *Angew. Chem.* **2020**, *132*, 1343–1349; c) P. Ji, X. Feng, P. Oliveres, Z. Li, A. Murakami, C. Wang, W. Lin, *J. Am. Chem. Soc.* **2019**, *141*, 14878–14888; d) C. G. Piscopo, C. M. Granadeiro, S. S. Balula, D. Bošković, *ChemCatChem* **2020**, *12*, 4721–4731.
- [11] a) H. Konnerth, B. M. Matsagar, S. S. Chen, M. H. G. Precht, F.-K. Shieh, K. C. W. Wu, *Coord. Chem. Rev.* **2020**, *416*, 213319; b) K. O. Otun, X. Liu, D. Hildebrandt, *J. Energy Chem.* **2020**, *51*, 230–245; c) D. Jampaiyah, D. Damma, A. Chalkidis, P. Venkataswamy, S. K. Bhargava, B. M. Reddy, *Catal. Today* **2020**, *356*, 519–526; d) N. Martín, A. Portillo, A. Ateka, F. G. Cirujano, L. Oar-Arteta, A. T. Aguayo, M. Dusselier, *ChemCatChem* **2020**, *12*, 5750–5758; e) X.-I. Wang, Y. Xiao, H. Yu, Y. Yang, X.-t. Dong, L. Xia, *ChemCatChem* **2020**, *12*, 5669–5678; f) S. Dou, S. Zhou, H. Huang, P. Yan, E. Shoko, T. T. Isimjan, X. Yang, *Chem. Eur. J.* **2020**, *26*, 16923–16931.
- [12] G. Hai, X. Jia, K. Zhang, X. Liu, Z. Wu, G. Wang, *Nano Energy* **2018**, *44*, 345–352.
- [13] a) Y. Zhao, W. Cai, M. Chen, Y. Bu, *J. Alloys Compd.* **2020**, *829*, 154508; b) Y. Pei, Z. Qi, X. Li, R. V. Maligal-Ganesh, T. W. Goh, C. Xiao, T. Wang, W. Huang, *J. Mater. Chem. A* **2017**, *5*, 6186–6192.
- [14] a) B. Wang, H. Huang, M. Huang, P. Yan, T. T. Isimjan, X. Yang, *Sci. China Chem.* **2020**, *63*, 841–849; b) Z. Wan, Q. He, J. Chen, T. T. Isimjan, B. Wang, X. Yang, *Chin. J. Catal.* **2020**, *41*, 1745–1753.
- [15] a) J. Guo, C. Wu, J. Zhang, P. Yan, J. Tian, X. Shen, T. T. Isimjan, X. Yang, *J. Mater. Chem. A* **2019**, *7*, 8865–8872; b) C. Wu, J. Guo, J. Zhang, Y. Zhao, J. Tian, T. T. Isimjan, X. Yang, *Renewable Energy* **2019**, *136*, 1064–1070.
- [16] a) F. Fu, C. Wang, Q. Wang, A. M. Martinez-Villacorta, A. Escobar, H. Chong, X. Wang, S. Moya, L. Salmon, E. Fouquet, J. Ruiz, D. Astruc, *J. Am. Chem. Soc.* **2018**, *140*, 10034–10042; b) J. Li, Q. Guan, H. Wu, W. Liu, Y. Lin, Z. Sun, X. Ye, X. Zheng, H. Pan, J. Zhu, S. Chen, W. Zhang, S. Wei, J. Lu, *J. Am. Chem. Soc.* **2019**, *141*, 14515–14519.
- [17] J. Guo, B. Wang, D. Yang, Z. Wan, P. Yan, J. Tian, T. T. Isimjan, X. Yang, *Appl. Catal. B* **2020**, *265*, 118584.
- [18] P. He, X.-Y. Yu, X. W. Lou, *Angew. Chem. Int. Ed.* **2017**, *56*, 3897–3900; *Angew. Chem.* **2017**, *129*, 3955–3958.
- [19] a) Y. He, S. Hwang, D. A. Cullen, M. A. Uddin, L. Langhorst, B. Li, S. Karakalos, A. J. Kropf, E. C. Wegener, J. Sokolowski, M. Chen, D. J. Myers, D. Su, K. L. More, G. Wang, S. Litster, G. Wu, *Energy Environ. Sci.* **2019**, *12*, 250–260; b) Z. Chen, R. Wu, Y. Liu, Y. Ha, Y. Guo, D. Sun, M. Liu, F. Fang, *Adv. Mater.* **2018**, *30*, 1802011.
- [20] A. Jawad, J. Lang, Z. Liao, A. Khan, J. Ifthikar, Z. Lv, S. Long, Z. Chen, Z. Chen, *Chem. Eng. J.* **2018**, *335*, 548–559.
- [21] H. Zhao, Z. Li, X. Dai, M. Cui, F. Nie, X. Zhang, Z. Ren, Z. Yang, Y. Gan, X. Yin, Y. Wang, W. Song, *J. Mater. Chem. A* **2020**, *8*, 6732–6739.
- [22] a) I. K. Mishra, H. Zhou, J. Sun, K. Dahal, S. Chen, Z. Ren, *Energy Environ. Sci.* **2018**, *11*, 2246–2252; b) R. Boppella, J. Tan, W. Yang, J. Moon, *Adv. Funct. Mater.* **2019**, *29*, 1807976; c) Y. Wang, G. Shen, Y. Zhang, L. Pan, X. Zhang, J.-J. Zou, *Appl. Catal. B* **2020**, *260*, 118183.
- [23] a) C. Wu, J. Zhang, J. Guo, L. Sun, J. Ming, H. Dong, Y. Zhao, J. Tian, X. Yang, *ACS Sustainable Chem. Eng.* **2018**, *6*, 7451–7457; b) Y. Liu, X. Li, Q. Zhang, W. Li, Y. Xie, H. Liu, L. Shang, Z. Liu, Z. Chen, L. Gu, Z. Tang, T. Zhang, S. Lu, *Angew. Chem. Int. Ed.* **2020**, *59*, 1718–1726; *Angew. Chem.* **2020**, *132*, 1735–1743.
- [24] C. Rajkumar, B. Thirumalraj, S.-M. Chen, P. Veerakumar, S.-B. Liu, *ACS Appl. Mater. Interfaces* **2017**, *9*, 31794–31805.
- [25] Z. Pu, J. Zhao, A. I. Saana, W. Li, M. Wang, D. He, S. Mu, *Energy Environ. Sci.* **2019**, *12*, 952–957.
- [26] X. Yang, A.-Y. Lu, Y. Zhu, M. N. Hedhili, S. Min, K.-W. Huang, Y. Han, L.-J. Li, *Nano Energy* **2015**, *15*, 634–641.
- [27] Y. Li, H. Wang, L. Xie, Y. Liang, G. Hong, H. Dai, *J. Am. Chem. Soc.* **2011**, *133*, 7296–7299.
- [28] a) P. Yan, M. Huang, B. Wang, Z. Wan, M. Qian, H. Yan, T. T. Isimjan, J. Tian, X. Yang, *J. Energy Chem.* **2020**, *47*, 299–306; b) B. Wang, H. Huang, T. Sun, P. Yan, T. T. Isimjan, J. Tian, X. Yang, *J. Colloid Interface Sci.* **2020**, *567*, 339–346.

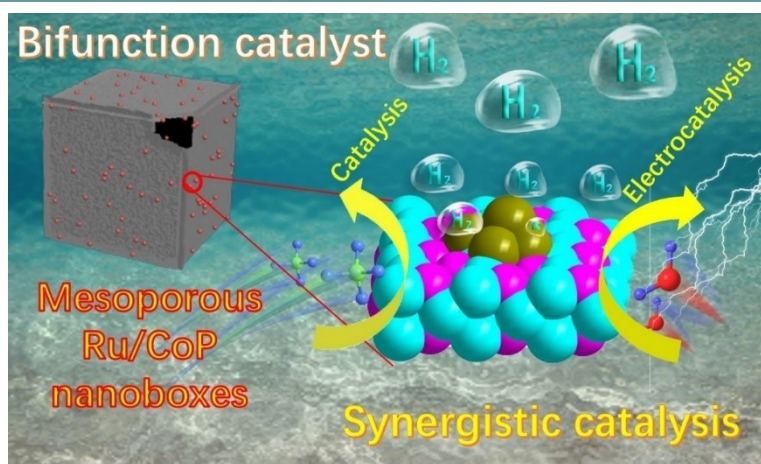
Manuscript received: May 26, 2021

Revised manuscript received: June 16, 2021

Accepted manuscript online: June 16, 2021

Version of record online:   

FULL PAPERS



S. Dou, C. Hu, L. Shi, W. Zhang, S. Zhou, P. Yan, Dr. L. D'Souza, Dr. T. T. Isimjan, Prof. X. Yang**

1 – 9

Well-Dispersed Ru-Clusters Decorating Nanobox-Structured CoP Synergistically Catalyze the NaBH₄ Hydrolysis and Electro-Reductive H₂ Evolution



Water splitting: A novel bifunctional Ru/CoP nanobox catalyst is fabricated by using ZIF-67 as the precursor. The resulting Ru/CoP catalyst exhibits

excellent activities for catalytic NaBH₄ hydrolysis and electrocatalytic H₂ evolution in alkaline media.